Electrically Small Huygens Antenna-Based Fully-Integrated Wireless Power Transfer and Communication System

Wei Lin, Member, IEEE and Richard W. Ziolkowski, Fellow, IEEE
University of Technology Sydney, Global Big Data Technologies Centre, Ultimo NSW 2007, Australia

Corresponding author: Wei Lin (e-mail: wei.lin@uts.edu.au).

This work was supported in part by the Australian Research Council grant number DP160102219 and UTS Chancellor's Postdoctoral Fellowship PRO18-6147.

ABSTRACT This paper introduces the first reported electrically small Huygens dual-functional wireless power transfer (WPT) and communication system operating in the 915 MHz ISM band. It is realized by the seamless combination of a Huygens linearly polarized (HLP) antenna and a highly efficient HLP rectenna. The configuration consists of two orthogonally oriented HLP subsystems. Each one intrinsically combines two pairs of metamaterial-inspired near-field resonant parasitic elements, i.e., an Egyptian axe dipole (EAD) and a capacitively loaded loop (CLL). Through the development of a very tightly coupled feed subsystem that includes the WPT mode's rectifier circuit and the communications mode's feedline while preserving their isolation, the independent operation of both functions is facilitated in an electrically small volume ($ka < 0.77$). The measured results of its fabricated prototype agree well with their simulated values. The communications mode antenna resonates at 910 MHz and radiates a cardioid-shaped Huygens pattern with the peak gain of 2.7 dBi. The Huygens-based WPT rectenna achieves an 87.2% peak AC to DC conversion efficiency at 907 MHz. The dual-functional system is an ideal candidate for many emerging Internet-of-Things (IoT) wireless applications that require simultaneous wireless information and power transfer (SWIPT) and wirelessly powered communications (WPC).

INDEX TERMS Dual-functional, electrically small antennas, Huygens radiation pattern, Internet-of-Things (IoT), rectenna, wireless power transfer

I. INTRODUCTION

Internet-of-Things (IoT) devices have been witnessing exponential growth in recent years. Their number is anticipated to reach 30 billion units by 2020 as we enter the 5G era [1], [2]. It has been recognized that it is impractical to power every IoT device with short-life batteries which would have to be charged or changed frequently. Consequently, far-field wireless power transfer (WPT) technologies are rapidly being developed to meet this 5G IoT need [3] – [5]. Moreover, because some IoT devices will be embedded into objects, such as a human body for biomedical sensor applications, WPT is the sole solution to power these devices [6].

These 5G trends have inspired new research areas on systems that provide simultaneous wireless information and power transfer (SWIPT) and wirelessly powered communications (WPC) [7] – [10]. SWIPT and WPC devices seek uninterrupted, ubiquitous wireless connectivity (UUWC) to achieve data transfer (one-way) and information exchanges (both ways). They require dual-functional antenna systems to enable both applications simultaneously. As an example, the IoT sensor network shown in Fig. 1 must sense the occurrence of a bush/forest fire and alert authorities to its location. Bush fires are a major natural disaster in Australia [11] and wireless sensors deployed to act as an early warning system would meet an important health and safety need. Dual-functional, compact wireless nodes are required for such a sensor network. Each node must be able to not only convert received wireless signals from a base station into DC energy to power up its sensor(s), but it must also facilitate the exchange of the resulting data with that station. However, the overall size of two separate antenna systems is impractical for compact IoT devices. Thus, dual-functionality in an electrically small package is highly desired. Nevertheless, it is challenging to realize.

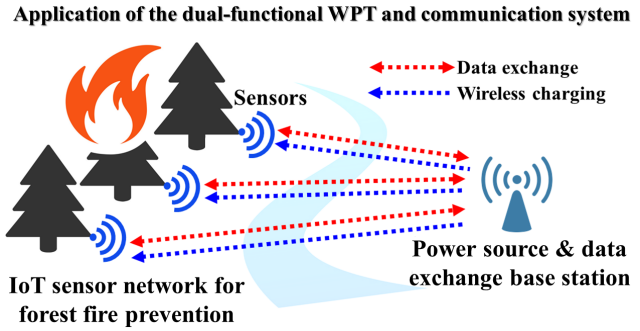

FIGURE 1. Example of the electrically small dual-functional WPT and communication system implemented as nodes in an IoT sensor network for application to bush and forest fire prevention.

In this paper, we present the first reported Huygens antenna-based fully-integrated WPT and communications system. This dual-functional device is realized in the 915 MHz ISM (Industrial, Scientific and Medical) band. High isolation between these two functions is demonstrated. The entire dual-functional system is electrically small, i.e., its $ka = 0.77 < 1.0$ (where a is the radius of the smallest sphere enclosing the entire antenna structure and $k = 2\pi/\lambda_0$ is the free-space wavenumber at the operational frequency [12]). It is also compact, its volume being only $\pi\,(0.25)^2 \times 0.07\,\lambda_0^3 = 0.014\,\lambda_0^3$. Cardioid-shaped Huygens radiation patterns with the peak realized gain of 2.7 dBi are achieved in both the communications and WPT mode. The rectenna's WPT function achieves an 87.2% peak AC to DC conversion efficiency. It is a low-cost, lightweight system; it is easily manufactured with standard PCB technology making its mass production feasible.

II. DESIGN METHODOLOGY

The dual-functional electrically small Huygens system is shown in Fig. 2(a). It is realized with two orthogonally polarized, electrically small HLP antennas. Each HLP antenna organically combines two metamaterial-inspired near-field resonant parasitic (NFRP) elements, an Egyptian axe dipole (EAD) and a capacitively loaded loop (CLL). The EAD acts as an electric radiator; the CLL acts as an orthogonal magnetic radiator in phase with the electric one. Their properly designed combination realizes cardioid-shaped Huygens radiation patterns. A detailed explanation of this class of Huygens dipole antennas is found in our previous works [13] – [15]. However, while these NFRP elements are of the same type as those employed in the mono-function, coax-fed circularly polarized (CP) antennas reported in [15], they had to be redesigned for their amalgamation with a uniquely developed subsystem that tightly integrates a rectifying circuit for the WPT function on receive and a feedline structure for the transmit-receive communications function. Moreover, while the orthogonal nature of the two HLP antennas yields excellent isolation between them in theory, this subsystem maintains the isolation in practice. As demonstrated in Fig. 2(b), it preserves the completely independent operation of both functions. Consequently, the dual-functional nature of the overall system is readily facilitated by its configuration.

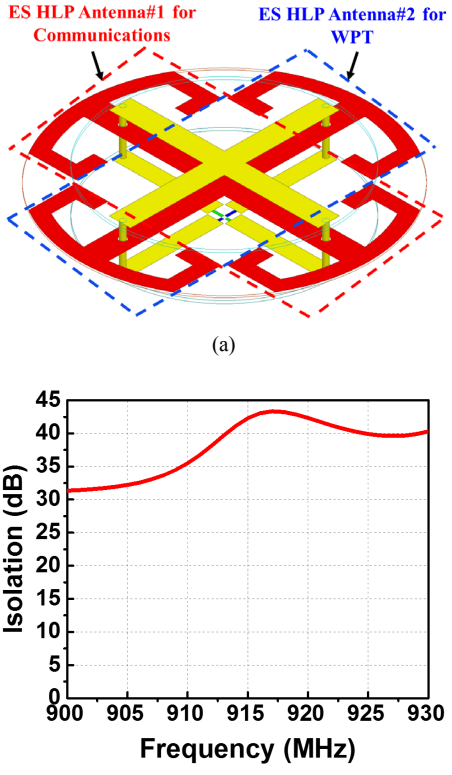

FIGURE 2. Electrically small, dual-functional WPT and communication system. (a) 3D view. (b) Simulated isolation between its functions.

III. REALIZATION AND PERFORMANCE

The configuration of the system is presented first. The antenna design was simulated and optimized with the ANSYS electromagnetics suite 16.2. The rectifying circuit was co-designed and optimized with the Agilent advanced design system (ADS). Its prototype was realized with standard PCB technology. The key design features that mitigate the coupling between the two functionalities are discussed next. Finally, the experimental results are analyzed.

A. SYSTEM CONFIGURATION

The dual-functional system is realized as shown in Fig. 3. It consists of four pieces of Rogers™ 5880 metal-cladded substrate ($\varepsilon_r = 2.2$, $\mu_r = 1.0$, $\tan\delta = 0.0009$ for the frequencies of interest). They are labeled as *substrate#1* to *substrate#4*. The thickness of substrate#2 is 0.508 mm; the thickness of the other three pieces is 0.7874 mm. The two orthogonal electrically small HLP elements, *HLP#1* and *HLP#2,* are oriented in a crossed, orthogonal formation. The orthogonal CLL elements, *CLL#1* and *CLL#2*, are fabricated in part on the top surfaces of *Substrate#1* and *Substrate#3*. These pieces are connected by four vertical cylindrical copper vias. They pass through circular holes in

the EAD elements without any electrical connection to them. The crossed EAD elements as *EAD#1* and *EAD#2* are etched on top surface of substrate#2 sandwiched by the CLL elements. The two short orthogonal dipoles that are associated with the two HLP elements are printed on the bottom layer of *Substrate#3*. The gap between the two arms of each short driven dipole is 1.0 mm.

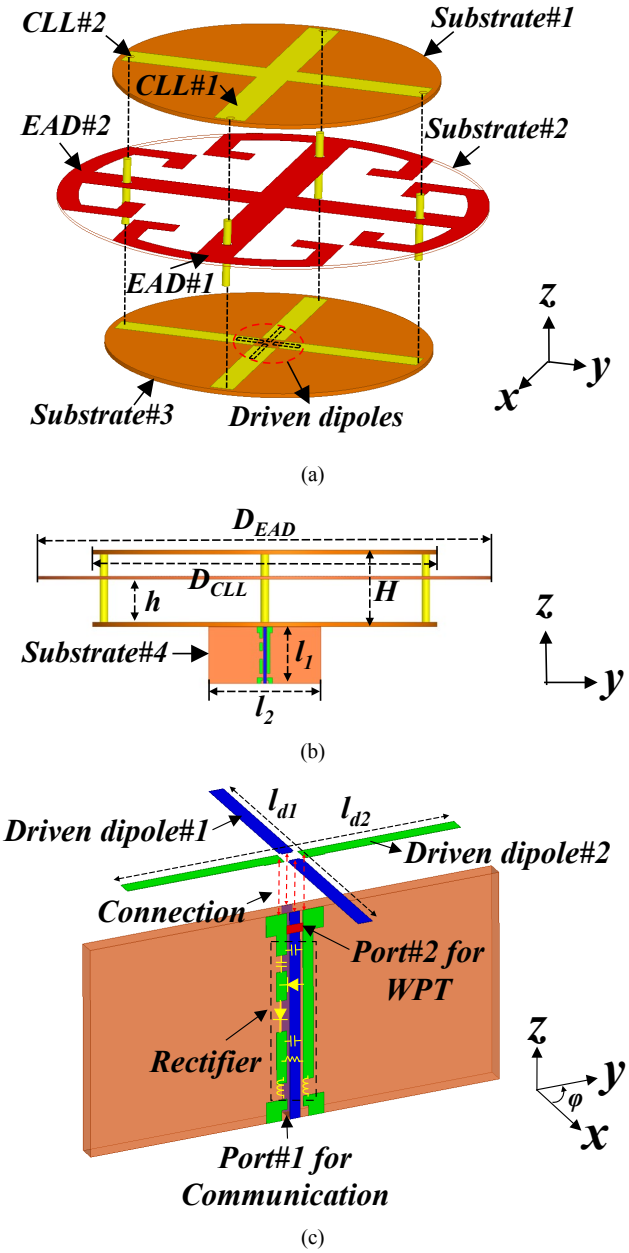

FIGURE 3. System configuration: (a) Perspective multilayer view of the entire system. (b) Side view. (c) Perspective view of the "driven" crossed-dipoles and the vertical substrate#4 that hosts the tightly integrated WPT rectifying circuit (see Fig. 8), the feedline of the communications subsystem, and their ports.

The *substrate#4* is attached to the bottom of *substrate*#3 through connections to the driven crossed-dipoles and is oriented orthogonal to it. It accommodates the parallel strip feedlines (~50 Ω impedance) etched on both sides of Substate#4 for the communications *HLP#1*. The coplanar strip lines of the AC-to-DC rectifier connected to the WPT *HLP#2* are etched on one side of substrate#4 in the yz-plane; the positive x-axis is normal to its face. The parallel feedline is extended for connection to a differential source. It could be readily modified to a ground-tapered balun for a SMA or coaxial cable connection. The rectifier is realized as a combination of lumped components as described in Section III.D below. The rectifying circuit and HLP#2 share a common port. The detailed parameters of the system are listed in Table I.

TABLE I:
SYSTEM DESIGN PARAMETERS (DIMENSIONS IN MILLIMETERS)

Parameter	Description	Value
D_{EAD}	Diameter of the whole system	80.8
D_{CLL}	Diameter of Substrate#1 and #3	61.4
h	Distance between Substrate#2 and #3	7.6
H	Height of the crossed HLP elements	13.6
l_1	Length of substrate#4 in z axis	10.0
l_2	Length of substrate#4 in y axis	20.0
l_{d1}	Length of the short driven dipole#1	15.8
l_{d2}	Length of the short driven dipole#2	16.3
d	Diameter of the copper post	1.5

B. KEY DESIGN CONSIDERATION

A key consideration in the design of the dual-Huygens LP system is the vertical orientation of the feedline and rectifier. Although substrate#4 would be avoided if the rectifier was deployed on the same plane as the crossed driven dipoles are, the radiation pattern from the communication mode deteriorates significantly. This is demonstrated in the Appendix.

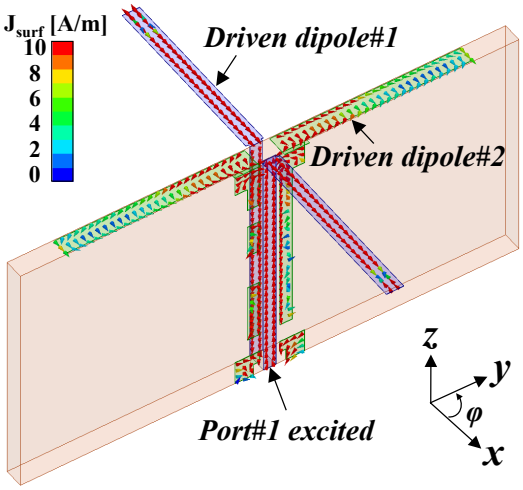

FIGURE 4. Current distributions on the entire feed structure if the system is in its communication mode with Port#1 being excited.

The currents on the crossed-dipoles and the lines on substrate#4 in the communications mode are shown in Fig. 4. Unlike the planar design and the current distributions on it that are shown in the Appendix, one clearly finds that

only minor currents are coupled onto the shorter driven dipoles of HLP#2 when Port#1 is excited. Thus, this orthogonal layout does satisfactorily prevent strong coupling between the components of the two modes. The resulting high isolation levels between the two modes, as shown in Fig. 2(b), facilitates achieving a very satisfactory Huygens radiation pattern in the communications mode.

C. EXPERIMENTAL RESULTS: COMM MODE

A prototype was fabricated and measured as illustrated in Fig. 5. A Keysight™ Vector Network Analyzer (VNA) was used to measure its $|S_{11}|$ values. A SATIMO Starlab near-field multi-probe system was used to measure its radiation patterns.

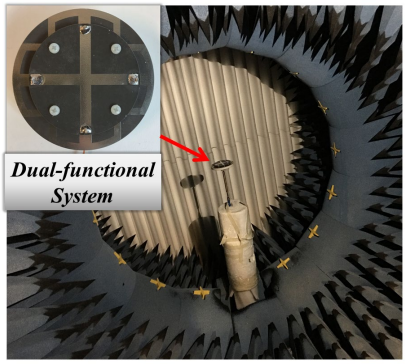

FIGURE 5. Multi-probe measurement of the dual-functional system in its communications mode.

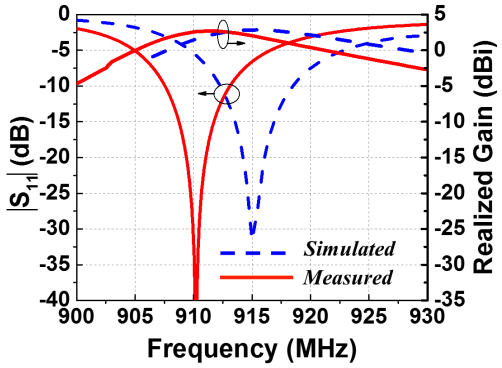

FIGURE 6. Measured and simulated $|S_{11}|$ and realized gain values of the dual-functional system in its communications mode as functions of the source frequency.

Fig. 6 shows the measured and simulated $|S_{11}|$ and realized gain values as functions of the source frequency. Very good agreement was achieved. The measured resonance frequency was 910 MHz, which was shifted only 5 MHz (0.5%) from its simulated value, 915 MHz. The peak realized gain, 2.7 dBi, was measured at the resonance frequency and is also reasonably close to its simulated value, 2.87 dBi. Typical fabrication, assembly, and measurement errors account for the differences that led to the noted 0.5% shift.

Fig. 7 presents the measured and simulated radiation patterns of the communications HLP mode at the resonance frequency in the two primary vertical planes (the pattern is essentially omnidirectional in the horizontal plane). The measured results again agree well with their simulated values. High quality Huygens radiation patterns are observed in both vertical planes. A large front-to-back-ratio (FTBR) value, 28.8 dB, was realized. Moreover, the measured 3-dB beamwidths are broad, 120° from -62° to 58° in the $\varphi = 0°$ plane and 135° from -63° to 72° in the $\varphi = 90°$ plane. Quite good Huygens radiation performance was thus confirmed for the communications mode.

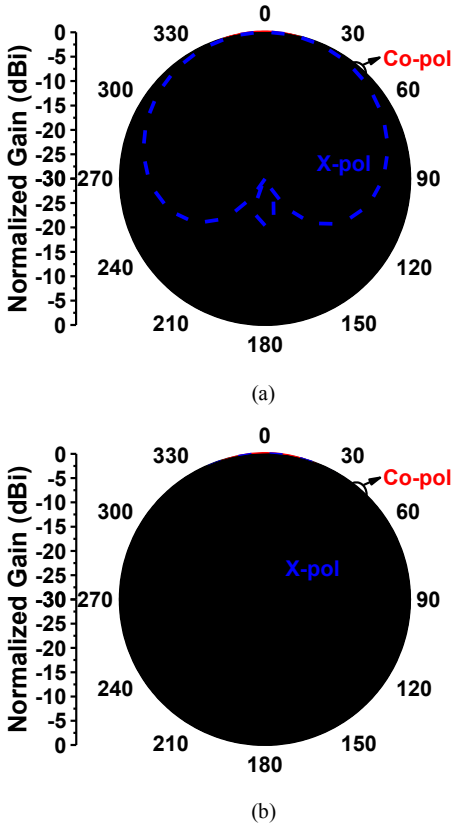

FIGURE 7. Measured and simulated radiation patterns of the dual-functional system in its communications mode at its center frequency in the two principal vertical planes. (a) $\varphi = 0°$. (b) $\varphi = 90°$.

D. EXPERIMENTAL RESULTS: WPT MODE

We note that unlike wireless power harvesting (WPH) rectennas [16] – [19], our rectenna system was designed specifically for intentional WPT [20] – [22]. Narrowband electrically small Huygens antennas are ideal candidates for this purpose. They are simpler and more compact since they do not require broadband or multiband receivers [23] – [25].

A highly efficient full-wave rectifying circuit was designed and implemented. Its circuit layout is shown in Fig. 8(a). A microscope image of the final rectifier prototype is shown in Fig. 8 (b). The entire structure is very compact; its length is only 1 cm. The circuit consists of an

inductor L; three capacitors: C_1, C_2 and C_3; two Schottky diodes; and a load resistor R_L. The inductor L and the capacitors C_1 and C_2 act as the impedance matching circuit. The inductor L also acts as a low pass filter to prevent the higher order harmonics generated from the non-linear diodes from being reradiated. The capacitor C_2 also works as the energy storage component during each negative period of the input sinusoidal signal. HSMS286C diodes package from Broadcom™ were adopted for this full-wave rectifier. Another capacitor C_3 smooths out the output DC voltage.

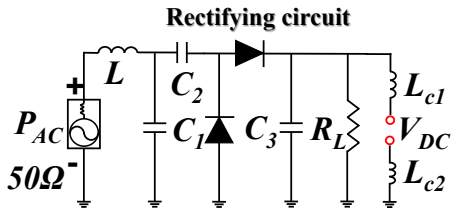

(a)

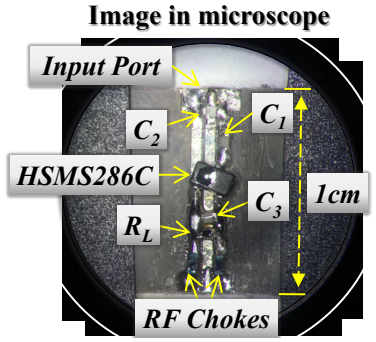

(b)

FIGURE 8. Rectifying circuit. (a) Layout. (b) Its implementation with lumped components (microscope view).

The rectifier alone was matched to and tested with a 50 Ω source. The matching inductor L was from Coilcraft™; the capacitors were from Murata™. The initial component values from simulation were L = 39 nH, R_L = 10 KΩ, C_1 = 0.4 pF, C_2 = 100 pF, and C_3 = 100 pF. The optimized values of the actual components were different: L = 22 nH and R_L = 5.1 KΩ, C_1 = 0.4 pF, C_2 = 100 pF, C_3 = 100 pF, due to a discrepancy between the actual values of the diodes and the company provided simulation model. Two 560 nH inductors were used as RF chokes. The simulated and actual impedance values are compared in the Smith-Chart plot in Fig. 9(a). It was determined from the first experiments that the matching L introduced considerably large losses. The circuit simulation results given in Fig. 9(b) demonstrate that the AC-to-DC efficiency decreases from 87.8% to 81.5% when the received power is 6 dBm if the lumped inductor is present in agreement with the measured results. The case "*without matching L*" is realized by assigning the impedance of the AC source to be an inductive value equivalent to L.

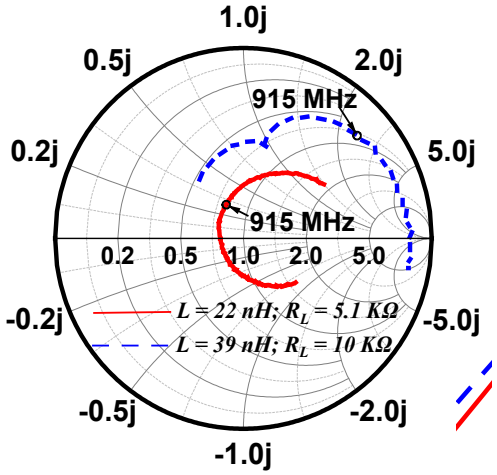

(a)

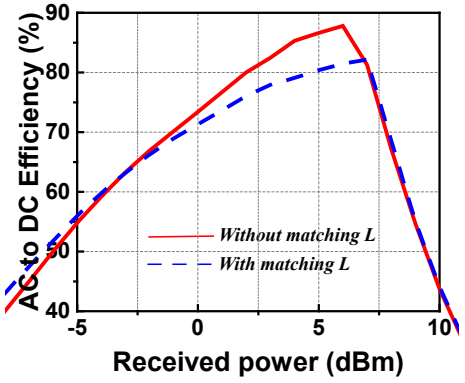

(b)

FIGURE 9. Rectifying circuit alone. (a) Measured impedance with different matching inductors: L = 22 nH and 39 nH. (b) Simulated AC-to-DC conversion efficiency with and without the matching inductor L = 39 nH.

Unlike in [15], the WPT's HLP antenna was not designed to be matched to a 50 Ω source. More importantly, it was designed to be matched directly to the impedance of the rectifying circuit, eliminating the inductor L. We found that this was simply accomplished by increasing the lengths of both of the HLP's dipoles a small amount, i.e., 15.8 mm for the communications and 16.3 mm for the WPT dipole elements. The input impedance then exhibits an inductive value (around 130 Ω) which nicely compensates the natural capacitive impedance of the rectifier. The reactance associated with the inductor, $X = j\omega L$ = j126 Ω, where L is the value of the inductance required for the 50 Ω match with the rectifying circuit at the resonance frequency, is provided now by the changes in the dipole lengths. This outcome is illustrated in Fig. 10(a). Again, the conversion efficiency enhancement with this direct (co-design) matching approach is highlighted in Fig. 9(b). Moreover,

the radiation patterns shown in Fig. 10(b) at the resonance frequency have the desired cardioid shape, i.e., the electric and magnetic NFRP elements are well-balanced. In comparison to rectennas based solely on an electric or a magnetic dipole antenna, the Huygens antenna provides twice the gain towards the source and minimizes any back radiation that could impact the performance of the rectifying circuit.

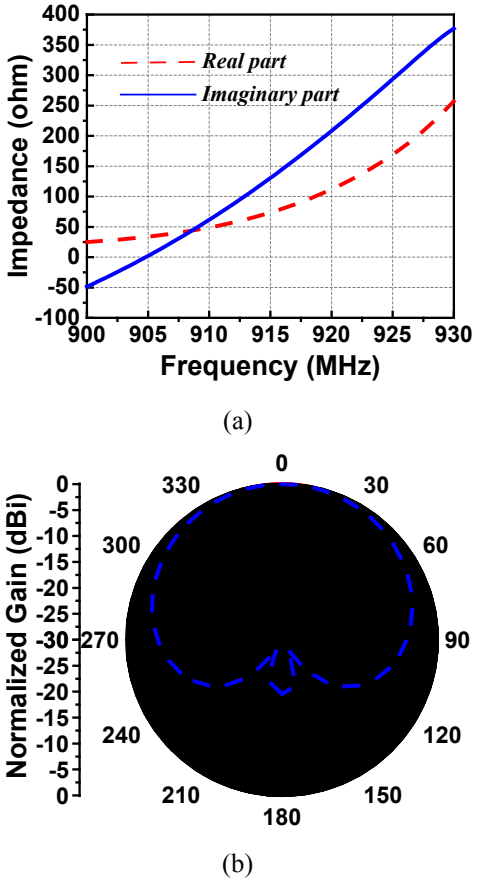

FIGURE 10. WPT HLP system. (a) Simulated impedance values. (b) Simulated radiation patterns at the resonance frequency, 915 MHz.

The rectenna mode was measured as shown in Fig. 11. A WPT measurement environment was set up, which consists of a signal generator to provide the power source, an amplifier with DC supplier to magnify the power, a horn antenna to produce the EM wave, two cables for connections, and a multimeter to measure the output DC voltage of the rectenna. All of the relevant parameters are given in Fig. 11. According to Friis transmission equation [26], we can control the magnitude of the wireless power illuminating the rectenna. The AC to DC efficiency is calculated in the standard manner [27] − [30] as the ratio between the measured output DC power to the incident wireless power.

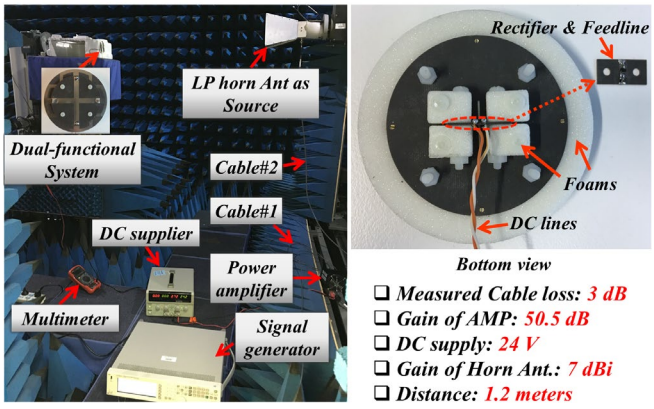

FIGURE 11. Rectenna measurement setup, the associated specifications, and a bottom view of the WPT HLP system.

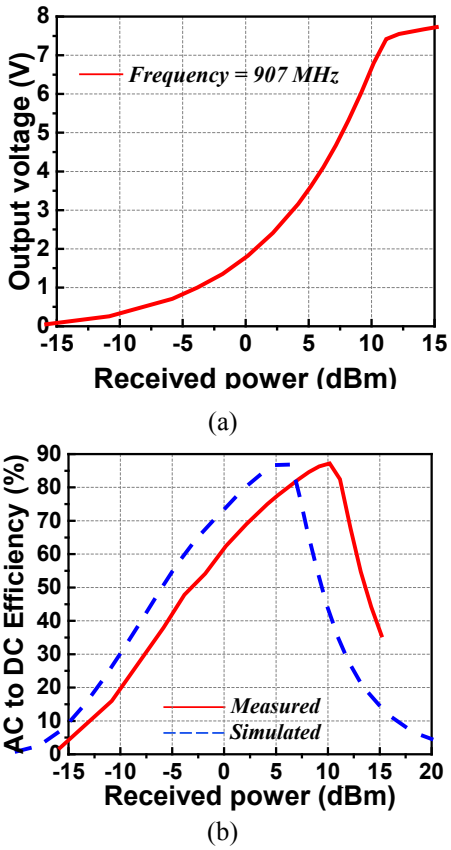

FIGURE 12. WPT HLP system. (a) Measured DC output voltage as a function of the received power and of the source frequency. (b) Measured and simulated AC-to-DC conversion efficiency.

The measured WPT results are shown in Fig. 12. First, we measured the output DC voltage values by sweeping the source frequency to find the one at which the rectenna produced the maximum value. This occurred at 907 MHz. The source frequency was then fixed at this value, and the output DC voltage was measured as a function of the incident power (calculated with the Friis transmission law

and the measurement system parameters given in Fig. 11). These results are shown in Fig. 12 (a). The output voltage begins to saturate at approximately 7.5 V. The output DC power reaches its maximum for 907 MHz when the received power is 8.2 dBm. The AC-to-DC conversion efficiency was then obtained. The measured and simulated values are compared in Fig. 12(b). It is clearly seen that the peak efficiency values: 87.2% for measurement and 87.8% for simulation, agree very well. Moreover, the trend of the measured and simulated results are also in reasonable agreement. The small observed frequency shift in them is again due to the small differences between the simulation model and the actual values of the Schottky diodes.

The modified cross-dipole-based rectenna-only WPT system reported in [25] operates in the same band. It has a measured *ka* = 1.66, a 1.8 dBi realized gain (RG), a 96° half-power beamwidth (HPBW), and a 0 dB FTBR. It achieved approximately a 65% conversion efficiency for the same incident power level. In comparison, our WPT system has the measured values: *ka* = 0.77, RG = 2.7 dBi, HPBW = 120°, and a 28.8 FTBR. It achieved an 87.2% conversion efficiency. Moreover, it is seamlessly integrated with the communications system.

IV. CONCLUSION

This paper presented the first developed electrically small Huygens fully-integrated, dual-functional wireless power transfer and communication system. The design methodology, system configurations and experimental results were described and discussed. The measured results confirmed the desired dual-functional performance of the system. It is an excellent candidate for a variety of anticipated wireless IoT applications.

REFERENCES

[1] C. -L. Hsu and J. C. -C. Lin, "An empirical examination of consumer adoption of Internet of Things services: Network externalities and concern for information privacy perspectives," *Comput. Human Behav.*, vol. 62, pp: 516–527, Sep. 2016.

[2] M. R. Palattella, et al., "Internet of things in the 5G era: Enablers, architecture, and business models," *IEEE J. Sel. Area. Commun.,* vol. 34, no. 3, pp. 510–527, Mar. 2016.

[3] N. B. Carvalho, et al., "Wireless power transmission: R&D activities within Europe," *IEEE Trans. Microw. Theory Techn.*, vol. 62, no. 4, pp. 1031-1045, Apr. 2014.

[4] N. Shinohara, "Beam control technologies with a high-efficiency phased array for microwave power transmission in Japan," *Proc. IEEE*, vol. 101, no. 6, pp. 1448-1463, Jun. 2013.

[5] A. Costanzo and D. Masotti, "Energizing 5G: Near- and far-field wireless energy and data transfer as an enabling technology for the 5G IoT," *IEEE Microw. Mag.*, vol. 18, no. 3, pp. 125-136, May 2017.

[6] T. Campi, S. Cruciani, F. Palandrani, V. De Santis, A. Hirata, and M. Feliziani, "Wireless power transfer charging system for AIMDs and pacemakers," *IEEE Trans. Microw. Theory Techn.*, vol. 64, no. 2, pp. 633-642, Feb. 2016.

[7] A. Costanzo, M. Dionigi, D. Masotti, M. Mongiardo, G. Monti, L. Tarricone, and R. Sorrentino, "Electromagnetic energy harvesting and wireless power transmission: A unified approach," *Proc. IEEE*, vol. 102, no. 11, pp. 1692-1711, Nov. 2014.

[8] S. Ulukus, A. Yener, E. Erkip, O. Simeone, M. Zorzi, P. Grover, and K. Huang, "Energy harvesting wireless communications: A review of recent advances," *IEEE J. Sel. Areas Commun.*, vol. 33, no. 3, pp. 360-381, Mar. 2015.

[9] S. Bi, C. K. Ho, and R. Zhang, "Wireless powered communication: Opportunities and challenges," *IEEE Commun. Mag.*, vol. 53, no. 4, pp. 117-125, Apr. 2015.

[10] K. Huang, C. Zhong, and G. Zhu, "Some new research trends in wirelessly powered communications," *IEEE Wireless Commun.*, vol. 23, no. 2, pp. 19 – 27, Apr. 2016.

[11] Information available [Online]: http://www.ga.gov.au/home.

[12] M. Gustafsson, C. Sohl, and G. Kristensson, "Illustrations of new physical bounds on linearly polarized antennas," *IEEE Trans. Antennas Propag.*, vol. 57, no. 5, pp. 1319–1327, May 2009.

[13] R. W. Ziolkowski, "Low profile, broadside radiating, electrically small Huygens source antennas," *IEEE Access*, vol. 3, pp. 2644-2651, Dec. 2015.

[14] M. C. Tang, H. Wang and R. W. Ziolkowski, "Design and testing of simple, electrically small, low-profile, Huygens source antennas with broadside radiation performance," *IEEE Trans. Antennas Propag.*, vol. 64, no. 11, pp. 4607–4617, Nov. 2016.

[15] W. Lin and R. W. Ziolkowski, "Electrically-small, low-profile, Huygens circularly polarized antenna," *IEEE Trans. Antennas Propag.*, vol. 66, no. 2, pp. 636-643, Feb. 2018.

[16] Z. Gu, S. Hemour, L. Guo, and K. Wu, "Integrated cooperative ambient power harvester collecting ubiquitous radio frequency and kinetic energy," *IEEE Trans. Microw. Theory Techn.*, vol. 66, no. 9, pp. 4178-4190, Sep. 2018.

[17] H. Sun, Y. X. Guo, M. He, and Z. Zhong, "Design of a high-efficiency 2.45-GHz rectenna for low-input-power energy harvesting," *IEEE Antennas Wireless Propag. Lett.*, vol. 11, pp. 929–932, 2012.

[18] H. Sun and W. Geyi, "A new rectenna using beamwidth-enhanced antenna array for RF power harvesting applications," *IEEE Antennas Wireless Propag. Lett.*, vol. 16, pp. 1451–1454, 2017.

[19] F. Erkmen, T. S. Almoneef, and O. M. Ramahi, "Electromagnetic energy harvesting using full-wave rectification," *IEEE Trans. Microw. Theory Techn.*, vol. 65, no. 5, pp. 1843-1851, May 2017.

[20] H. Matsumoto, "Research on solar power satellites and microwave power transmission in Japan," *IEEE Microw. Mag.*, vol. 3, no. 4, pp. 36-45, Dec. 2002.

[21] R. M. Dickson, "Power in the sky: Requirements for microwave wireless power beamers for powering high-altitude platforms," *IEEE Microw. Mag.*, vol. 14, pp. 36-47, Apr. 2013.

[22] Z. Popovic, "Cut the cord: Low-power far-field wireless powering," *IEEE Microw. Mag.*, vol. 14, no. 2, pp. 55-62, Mar. 2013.

[23] V. Palazzi, et al., "A novel ultra-lightweight multiband rectenna on paper for RF energy harvesting in the next generation LTE bands," *IEEE Trans. Microw. Theory Techn.*, vol. 66, no. 1, pp. 366-379, Jan. 2018.

[24] S. Shen, C.-Y. Chiu, and R. D. Murch, "Multiport pixel rectenna for ambient RF energy harvesting," *IEEE Trans. Antennas Propag.,* vol. 66, no. 2, pp. 644-656, Feb. 2018.

[25] C. Song, Y. Huang, J. Zhou, P. Carter, S. Yuan, Q. Xu, and Z. Fei, "Matching network elimination in broadband rectennas for high-efficiency wireless power transfer and energy harvesting," *IEEE Trans. Industrial Electron.*, vol. 64, no. 5, pp. 3950-3961, May 2017.

[26] C. A. Balanis, 3rd Ed., *Antenna Theory*. New York: John Wiley & Sons, 2005.

[27] S.-T. Khang, D.-J. Lee, I.-J. Hwang, T.-D. Yeo, and J.-W. Yu, "Microwave power transfer with optimal number of rectenna arrays for midrange applications," IEEE Antennas Wirel. Propag. Lett., vol. 17, no. 1, pp. 155 – 159, Jan. 2018.

[28] M. Mattsson, C. I. Kolitsidas, and B. L. G. Jonsson, "Dual-band dual-polarized full-wave rectenna based on differential field sampling," IEEE Antennas Wirel. Propag. Lett., vol. 17, no. 6, pp. 956 – 959, Jun. 2018.

[29] Y. Yang, J. Li, L. Li, Y. Liu, B. Zhang, H. Zhu, K. Huang, "A 5.8 GHz circularly polarized rectenna with harmonic suppression and rectenna array for wireless power transfer," IEEE Antennas Wirel. Propag. Lett., vol. 17, no. 7, pp. 1276 – 1280, Jul. 2018.

[30] C. Liu, Y. X. Guo, H. Sun, and S. Xiao, "Design and safety considerations of an implantable rectenna for far-field wireless power transfer," *IEEE Trans. Antennas Propag.*, vol. 62, no. 11, pp. 5798–5806, Nov. 2014.

APPENDIX: Feed System Design

The configuration in which the rectifier was placed on the same plane as the driven element of the communication system was investigated to decrease the profile of the dual-functional system. Figures A.1 to A.3 depict the simulated results. The configuration is shown in Fig. A.1. The corresponding simulated current distributions on the feed structure and associated driven dipole elements when either Port#1 or Port#2 is excited are given in Fig. A.2. It is clearly observed that strong currents will be coupled to the strip lines of the rectifier and the driven dipole of HLP#2 if Port#1 is excited, i.e., in the communications mode. Consequently, as illustrated in Fig. A.3, this coupling causes the serious degradation of the communications mode's radiation pattern away from the desired cardioid-shaped Huygens pattern. On the other hand, it is also seen that only minor currents will be induced by this coupling on the short driven dipole of HLP#1 if Port#2 is excited. Consequently, a good Huygens radiation patterns will still be realized for the WPT mode. Since this planar design strongly affected the radiation performance of the communications mode when Port#1 was excited, the orthogonal substrate piece design on which the feed lines and rectifier resides was developed to attain the final optimized dual-functional design.

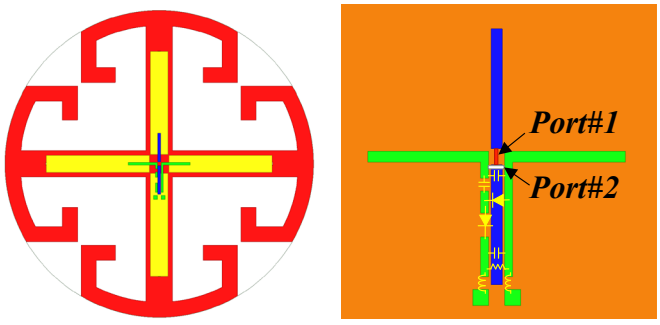

FIGURE A1. Design of rectifier located in the same plane of the crossed driven dipole (a) Overall view. (b) Enlarged view of the feed structure.

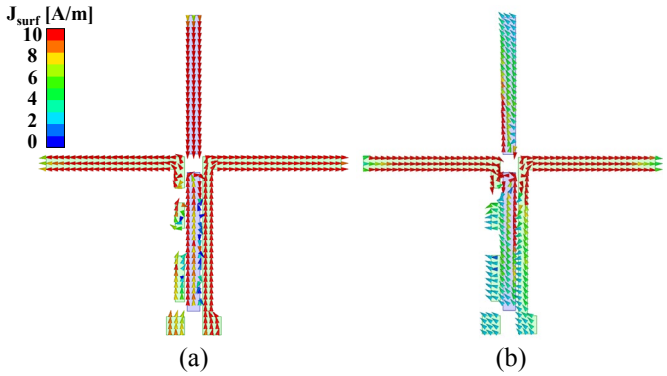

FIGURE A.2 Current distributions on the feed structure. (a) Port#1 is excited. (b) Port#2 is excited.

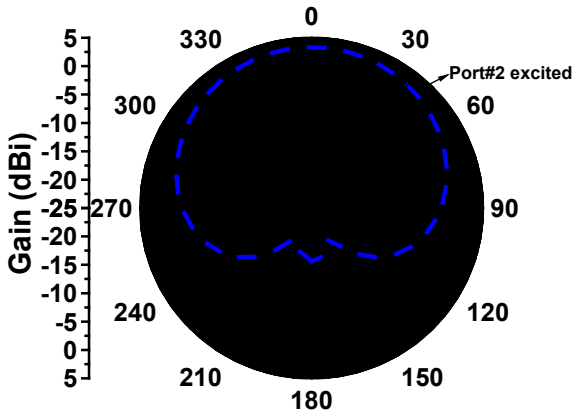

FIGURE A.3. Radiation patterns of the design where rectifier is deployed in the same plane of the driven dipoles.

Wei LIN received his PhD degree in Electronic Engineering from City University of Hong Kong, Hong Kong SAR in August 2016. He received the Master and Bachelor degrees, both in Electronic Engineering, at the South China University of Technology, Guangzhou, China in July 2012 and July 2009, respectively. He worked as a Research Associate at the Nanyang Technological University, Singapore from August 2012 to August 2013 and as a Postdoc Research Associate at University of Technology Sydney, Australia from October 2016 to September 2018.

Dr. Lin is currently a Chancellor's Postdoctoral Research Fellow with the Global Big Data Technologies Centre, School of Electrical and Data Engineering, University of Technology Sydney, Ultimo NSW, Australia. Dr. Lin received many academic awards, which mainly include the Best Paper Award (First Prize) at the *International Symposium on Antennas and Propagation (ISAP 2018)*; the Best Young Professional Paper Award (First prize) at the *3rd Australian Microwave Symposium (AMS2018)*; the Best Poster Paper Award at *the 2nd international conference on Electromagnetic Materials and Technologies for the Future (EM-MTF2017)*; a Talent Development Scholarship from the Hong Kong Government; and the Young Scientist Award at the *IEEE Region 10 conference (TENCON2015)*. Dr. Lin was the recipient of the 2018 UTS Early Career Researcher Grant Award and 2019 UTS Chancellor's Postdoctoral Research Fellowship. He serves as reviewers for several IEEE and IET journals and received the Outstanding Reviewer Award for *IEEE Antennas and Wireless Propagation Letters* in July 2018.

His research interests include the designs of circularly polarized antennas, electrically small antennas, reconfigurable antennas, HF antennas, satellite antennas, millimeter wave antennas, wireless power transfer, terahertz devices, and their applications.

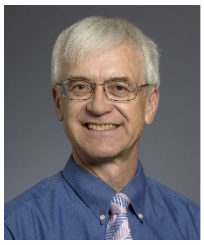

Richard W. Ziolkowski received the B.Sc. (magna cum laude) degree (Hons.) in physics from Brown University, Providence, RI, USA, in 1974; the M.S. and Ph.D. degrees in physics from the University of Illinois at Urbana-Champaign, Urbana, IL, USA, in 1975 and 1980, respectively; and the Honorary Doctorate degree from the Technical University of Denmark, Kongens Lyngby, Denmark in 2012.

He is currently a Distinguished Professor in the Global Big Data Technologies Centre in the Faculty of Engineering and Information Technologies (FEIT) at the University of Technology Sydney, Ultimo NSW, Australia. He became a Professor Emeritus at the University of Arizona in 2018, where he was a Litton Industries John M. Leonis Distinguished Professor in the Department of Electrical and Computer Engineering in the College of Engineering and was also a Professor in the College of Optical Sciences. He was the Computational Electronics and Electromagnetics Thrust Area Leader with the Lawrence Livermore National Laboratory, Engineering Research Division, in Livermore, CA before joining The University of Arizona, Tucson, AZ, USA, in 1990.

Prof. Ziolkowski is the recipient of the 2019 IEEE Electromagnetics Award (IEEE Field Award). He is a Fellow of the Optical Society of America (OSA, 2006), and of the American Physical Society (APS, 2016). He was the Australian DSTO Fulbright Distinguished Chair in Advanced Science and Technology from 2014-2015. He was a 2014 Thomas-Reuters Highly Cited Researcher. He served as the President of the IEEE Antennas and Propagation Society in 2005. He is also actively involved with the URSI, OSA and SPIE professional societies.

His current research interests include the application of new mathematical and numerical methods to linear and nonlinear problems dealing with the interaction of electromagnetic and acoustic waves with complex linear and nonlinear media, as well as metamaterials, metamaterial-inspired structures, nano-structures, and other classical and quantum applications-specific configurations.